# Timescales of Quartz Crystallization and the Longevity of the Bishop Giant Magma Body

# Guilherme A. R. Gualda<sup>1</sup>\*, Ayla S. Pamukcu<sup>1</sup>, Mark S. Ghiorso<sup>2</sup>, Alfred T. Anderson Jr<sup>3</sup>, Stephen R. Sutton<sup>3,4</sup>, Mark L. Rivers<sup>3,4</sup>

1 Vanderbilt University, Earth & Environmental Sciences, Nashville, Tennessee, United States of America, 2 OFM Research - West, Seattle, Washington, United States of America, 3 The University of Chicago, Geophysical Sciences, Chicago, Illinois, United States of America, 4 The University of Chicago, Center for Advanced Radiation Sources, Argonne, Illinois, United States of America

# Abstract

Supereruptions violently transfer huge amounts (100 s–1000 s km<sup>3</sup>) of magma to the surface in a matter of days and testify to the existence of giant pools of magma at depth. The longevity of these giant magma bodies is of significant scientific and societal interest. Radiometric data on whole rocks, glasses, feldspar and zircon crystals have been used to suggest that the Bishop Tuff giant magma body, which erupted ~760,000 years ago and created the Long Valley caldera (California), was long-lived (>100,000 years) and evolved rather slowly. In this work, we present four lines of evidence to constrain the timescales of crystallization of the Bishop magma body: (1) quartz residence times based on diffusional relaxation of Ti profiles, (2) quartz residence times based on the kinetics of faceting of melt inclusions, (3) quartz and feldspar crystallization times derived using quartz+feldspar crystal size distributions, and (4) timescales of cooling and crystallization based on thermodynamic and heat flow modeling. All of our estimates suggest quartz crystallization on timescales of <10,000 years, more typically within 500–3,000 years before eruption. We conclude that large-volume, crystal-poor magma bodies are ephemeral features that, once established, evolve on millennial timescales. We also suggest that zircon crystals, rather than recording the timescales of crystallization of a large pool of crystal-poor magma, record the extended periods of time necessary for maturation of the crust and establishment of these giant magma bodies.

Citation: Gualda GAR, Pamukcu AS, Ghiorso MS, Anderson AT Jr, Sutton SR, et al. (2012) Timescales of Quartz Crystallization and the Longevity of the Bishop Giant Magma Body. PLoS ONE 7(5): e37492. doi:10.1371/journal.pone.0037492

Editor: Nicolas Houlie, University of Leeds, United Kingdom

Received June 22, 2011; Accepted April 24, 2012; Published May 30, 2012

**Copyright:** © 2012 Gualda et al. This is an open-access article distributed under the terms of the Creative Commons Attribution License, which permits unrestricted use, distribution, and reproduction in any medium, provided the original author and source are credited.

**Funding:** Support was provided by NSF to ATA (EAR-0408707), GARG (EAR-0948528) and MSG (EAR-0948734). Portions of this work were performed at GeoSoilEnviroCARS (Sector 13), Advanced Photon Source (APS), Argonne National Laboratory; GeoSoilEnviroCARS is supported by NSF (EAR-0622171) and Department of Energy–Geosciences (DE-FG02-94ER14466); use of the Advanced Photon Source was supported by the U. S. Department of Energy, Office of Science, Office of Basic Energy Sciences (Contract No. DE-AC02-06CH11357). The funders had no role in study design, data collection and analysis, decision to publish, or preparation of the manuscript.

Competing Interests: The authors have declared that no competing interests exist.

\* E-mail: g.gualda@vanderbilt.edu

# Introduction

Supereruptions [1] provide compelling evidence that giant bodies of low-density, crystal-poor magma - larger than currently known magma bodies (see [2]) - existed just a few kilometers below the surface. The generation of such large pools of magma and their eruption are fascinating phenomena from a scientific standpoint, but also constitute a major threat to humanity [1,3]. Our knowledge of the processes and consequences related to these events is limited, largely because the last known supereruption on Earth occurred ca. 26,000 years ago [1]. The 1815 eruption of Tambora – the largest known historic eruption – led to the "Year without a summer" in North America and Europe in 1816 [4]. Yet, the Bishop supereruption, which took place  $\sim$ 760,000 years ago and created the Long Valley caldera in California [5–7], ejected at least an order of magnitude more magma, demonstrating that these giant eruptions can not only cause widespread devastation at the local scale, but can also have a significant worldwide impact, particularly on climate [1,3].

The longevity of giant magma bodies has generated continued interest [8,9]; the Bishop Tuff, in particular, has been the focus of numerous studies using age-dating (for a recent review, see [10]).

One of the continuing puzzles is that the timescales inferred are not always consistent with each other [10,11]. While ion probe U-Pb zircon ages suggest zircon crystallization over >100 ka [10], whole-grain TIMS U-Pb zircon ages combined with Ar-Ar sanidine eruption ages suggest millennial timescales [11]; however, the latter results critically depend on the intercomparability of U-Pb and Ar-Ar ages, a point of significant contention [12].

In discussion here is also the potential geological significance of the various results. What are the timescales of assembly of a giant magma body? What are the timescales of crystallization of such a magma body? The challenge is that the timescales of interest are largely inaccessible to geochronology for deposits as old as the youngest supercruptions. These timescales are accessible, however, using kinetic markers of magmatic processes (i.e. geospeedometers, see [13]). We present here direct evidence of the timescales of quartz crystallization in the Bishop Tuff magma body, and we compare these timescales to those expected from simple thermodynamic and heat flow calculations. Our results shed light onto the questions above and have significant implications for the timescales over which eruptible crystal-poor magma resides in the upper crust.

#### **Materials and Methods**

#### Samples

Our sample set includes 6 pumice clasts from the Chalfant Quarry in the southeastern portion of the Bishop Tuff [14,15], and 5 pumice clasts from the Aeolian Buttes in the northern portion of the deposit [16]. In the stratigraphic classification scheme of Wilson & Hildreth [7], our samples derive from fall unit F7 (2 pumice clasts), fall unit F8 (1), ash-flow unit Ig2Ea (3), and ash-flow unit Ig2NWb (5).

Studied samples encompass much of the spectrum of pumice density, porosity, crystallinity and textural variations observed in the Bishop Tuff as a whole [14]. Crystal size distributions for the samples from Chalfant were previously determined by us [14,15], and we discuss recent results on crystal size distributions for samples of the Aeolian Buttes [16,17]. Quartz zoning data presented here are exclusively for samples from Chalfant. Melt inclusion shape information derives from observations partly reported by Anderson et al. [18].

#### Analytical methods

Samples were studied using a combination of (for details, see [19]):

- (1) Documentation of sizes and shapes of whole quartz crystals and their melt inclusions; we place whole crystals in refractive index oil (so as to emphasize the inclusions), and we make observations under a petrographic microscope; over the years, we have inspected hundreds of crystals, each one containing tens of inclusions, so we have made qualitative observations on thousands of inclusions; we have only characterized in detail a small number of inclusions;
- (2) Cathodoluminescence (CL) imaging of individual quartz crystals (~100 in total) by electron microprobe at The University of Chicago, using methods similar to those of Peppard et al. [20];
- (3) Trace-element analysis at low spatial resolution (~25 μm) by laser ablation mass spectrometry (LA-ICPMS);
- (4) Trace-element analysis along traverses and 2D maps (4 crystals studied) at high spatial resolution (ca. 2–10  $\mu$ m spacing) using synchrotron x-ray microfluorescence (x-ray microprobe; see [21]) at the GeoSoilEnviroCARS insertion device beamline at the Advanced Photon Source (Argonne National Lab); the x-ray microprobe uses a highly collimated, synchrotron-based x-ray beam to generate characteristic x-ray spectra with very low background, which yields  $2\sigma$  uncertainty close to 2.5% for ca. 50 ppm Ti in quartz, using a 5  $\mu$ m spot [21];
- (5) X-ray tomography of pumice chips at various resolutions (2.5 to 15 μm per voxel), performed at the GeoSoilEnviroCARS bending magnet beamline, using methods described elsewhere [15,16].

# **MELTS** calculations

Our ongoing effort to use MELTS to model the evolution of silicic systems has shown that the current calibration of MELTS [22] fails to correctly predict the quartz+feldspar saturation surface as a function of pressure. We recently developed a new calibration of MELTS, rhyolite-MELTS, optimized for fluid-bearing rhyolitic magmas [23]. Our calibration takes advantage of the overwhelming evidence for simultaneous saturation of quartz, sanidine, and plagioclase in early-erupted Bishop pumice, and the wellconstrained pressure and fluid phase composition and abundance from melt inclusions [24,25]. Our tests indicate that the corrections lead to much improved results not only for Bishop magma, but also for other silicic systems [23].

We use rhyolite-MELTS to constrain the crystallization paths, and, in particular, the heat of cooling and crystallization for compositions relevant for the Bishop Tuff. We use early- and lateerupted bulk pumice (from [6]) and melt inclusion (from [18]) compositions. Calculations using the H<sub>2</sub>O-CO<sub>2</sub> solubility model of Papale et al. [26] show that both early- and late-erupted melt inclusion compositions yield fluid-saturation under the conditions inferred [24,25]. Unfortunately, we are currently unable to model a H<sub>2</sub>O-CO<sub>2</sub> fluid phase; however, the solubility of CO<sub>2</sub> in melts is so low [27] that the phase relations are virtually unchanged [28,29]. Accordingly, in our simulations, we add H<sub>2</sub>O to the initial compositions until rhyolite-MELTS calculates fluid saturation; the effect is that the activity of water in the melt is buffered throughout crystallization, as would be the case in the presence of a H<sub>2</sub>O-CO<sub>2</sub> fluid (for a more extended discussion, see [23]).

Crystallization pressure is determined using rhyolite-MELTS as the pressure at which melt inclusion compositions show simultaneous crystallization of quartz+sanidine+plagioclase under fluidsaturated conditions (see [23]).

## Results

#### Timescales of quartz crystallization

To assess the timescales of quartz crystallization and their implications for the longevity of giant rhyolitic magma bodies, we analyze three lines of evidence: (1) quartz residence times based on the diffusional relaxation of Ti zoning profiles; (2) melt inclusion faceting timescales, over which initially round melt inclusions attain partly faceted shapes; (3) quartz+feldspar crystallization times as recorded in crystal size distributions. We discuss the theory behind residence time and melt inclusion faceting timescale calculation in some detail, and highlight the connection of these results with those obtained using crystal size distributions, which are detailed elsewhere [16,17].

Diffusional relaxation times. Quartz crystals are characterized by a volumetrically predominant low-Ti (~40 ppm Ti) interior portion (Fig. 1). A small fraction (<10%) of crystals also include a relatively high-Ti (~50 ppm Ti) central core (50-100 µm in diameter); in the absence of such a core, the interior portion extends to the center of the observed crystal section. Finally, a variable proportion of crystals show a 50-100 µm thick rim with high Ti ( $\sim$ 50 ppm Ti), which corresponds to the bright cathodoluminescence (CL) rims first recognized by Peppard et al. [20]. Similar rims are observed on sanidine crystals. The origin of such features is contentious, and to what extent they record replenishment of the magma body [30,31], sinking of phenocrysts [18], or decompression of the system [19,32] is yet to be established. Nonetheless, quartz crystallization timescales can be inferred using diffusional relaxation times of Ti zoning in quartz from early-erupted Bishop pumice (Fig. 1).

Residence time calculation. The sharpness of contacts between chemically distinct zones in crystals can constrain the residence times of these internal contacts, and the durations and rates of crystal growth. The rationale is that once established, concentration gradients tend to relax by diffusion (e.g. [33]); diffusivities are such that relaxation is significant while at magmatic conditions, but becomes negligible after eruption, such that timescales and rates relevant to magmatic processes can be retrieved. In the present case, the problem is particularly simple because quartz has uniform major element composition, and there is no need to

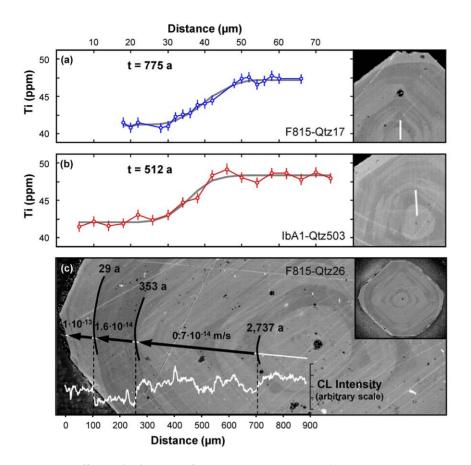


**Figure 1. Diffusional relaxation of Ti in quartz.** (a–b) X-ray profiles and cathodoluminescence (CL) images of select quartz crystals with bright-CL, high-Ti cores; residence times and growth rates derived from Ti traverses (white lines) are presented. Analytical points shown by open symbols, including analytical uncertainties (bars). Best fit curve (Equation 1) is shown in gray, calculated so as to minimize the sum of the squares of the difference between calculated and observed values. Calculated residence times are also shown. (c) CL image detailing core-rim zoning of a large quartz crystal; image of whole crystal shown in inset. White line corresponds to the location of CL traverse displayed in the bottom, with contacts between different zones indicated in black. Residence times in years and derived growth rates indicated by numbers on top of arrows. Notice that innermost contact has residence time close to 3,000 years. Calculated growth rates for two interior zones are close to  $10^{-14}$  m/s, while growth rate doi:10.1371/journal.pone.0037492.g001

consider potential effects of composition on the partition or diffusion coefficients.

Diffusion of Ti in quartz is particularly useful for the problem of interest here, as (1) diffusion rates have been determined experimentally (i.e.  $D_{Ti}^{Qtz} = 8.05 \times 10^{-22} \text{ m}^2 \text{ s}^{-1}$  at 750°C; see [34]), and are adequate to constrain timescales in question; and (2) Ti contents in quartz, in concentrations of 10 s of ppm, while not trivial to measure, can be measured with sufficient precision at the micrometer scale using the x-ray microprobe. Because large variations in Ti concentration in quartz correlate well with large changes in CL intensity [19,35], CL images and profiles can, in favorable instances, be used as a proxy for Ti variations. We use both Ti profiles obtained using the x-ray microprobe and CL intensity profiles derived from CL images, which allows us to study a larger number of crystals than would be possible with Ti profiles alone. Profiles were selected so as to be approximately orthogonal to the contact between different zones; departures from orthogonality are small and their effect on calculated times can be effectively neglected.

We use a 1D diffusion model to determine the time interval during which two zones of distinct compositions within a crystal were in contact with each other. We call this the contact residence time. We assume constant but different initial compositions in the two zones of the crystal at time t = 0. The predicted composition c(x) as a function of position x along the profile is described by [36]:

$$\mathbf{c}(\mathbf{x}) = \frac{1}{2} \operatorname{erfc}\left(\frac{\mathbf{x} - \mathbf{x}_{c}}{2\sqrt{\mathrm{Dt}}}\right) * \left[\mathbf{c}(-\infty) - \mathbf{c}(+\infty)\right] + \mathbf{c}(+\infty) \quad (1)$$

where erfc is the complementary error function,  $x_c$  is the position of the initial contact between the two zones (e.g. the position of the initial jump in composition), D is the diffusion coefficient, t is time, and  $L=2\sqrt{Dt}$  is the characteristic diffusion length scale. The predicted composition described by Equation 1 is fit to the observations by iteratively adjusting  $x_c$ ,  $c(-\infty)$ ,  $c(+\infty)$ , and L so as to minimize the sum of the squares of the differences (SSD) between observed and predicted composition. Using the known diffusivity D, we infer the diffusion time from the best-fit value of L. This fitting procedure makes it possible to recover estimates of L that are smaller than the spacing of the profile. We test whether L is appropriately resolved by varying its value about the best-fit value; when the sum of the square of the differences between observed and fitted curves increases with both larger and smaller values of L, we conclude that the diffusion time is resolved, even if L is smaller than the sampling interval; alternatively, this test may

show that reduction of the diffusion distance leads to no change in the SSD, and the obtained value is simply a maximum estimate.

*Error propagation.* It is of great interest to assess the errors associated with the calculated residence times. In order to derive an expression for the uncertainties associated with the residence time t, we re-write the equation  $L = 2\sqrt{Dt}$  as an explicit function of temperature (T) by using the Arrhenius relation  $D = D_o \exp [-E/RT]$ ):

$$t = \frac{L^2}{4D_o \exp(-E/RT)}$$
(2)

where  $D_o$  is the pre-exponential factor and E is the activation energy for diffusion, both of which have been determined experimentally [34]. Error propagation shows that:

$$\left(\frac{\sigma_{t}}{t}\right)^{2} = \left(\frac{E}{RT}\right)^{2} \left[\left(\frac{\sigma_{E}}{E}\right)^{2} + \left(\frac{\sigma_{T}}{T}\right)^{2}\right] + \left(2\frac{\sigma_{L}}{L}\right)^{2} + \left(\sigma_{\ln[D_{0}]}\right)^{2} \quad (3)$$

Uncertainties on E and  $ln(D_0)$  come directly from experiments (i.e.  $E = 273 \pm 12 \text{ kJ mol}^{-1}$ ,  $\sigma_E / E = 4.4\%$ ,  $\log[D_0] = -7.154 \pm 0.525$ ,  $\sigma_{\ln[D0]} = 1.2$ ; see [34]), while the other parameters have to be estimated. Best estimates for the crystallization temperature of the Bishop magma are in the range 720–780°C [6,37]. We choose a temperature of 750°C, and an uncertainty of  $15^{\circ}C$  (1 $\sigma$ ), such that the resulting 95% confidence interval matches the estimated T range. This calculation yields  $\sigma_T/T = 1.5\%$ , much smaller than the other contributions. Uncertainties on L derive from the fitting procedure. For Ti profiles, a Monte Carlo procedure was used to estimate the effect of the uncertainty at each point on L, which results in estimated errors in L of ca. 10-50%. Because the focus is not on the individual dates, but rather on the best estimate for the age of a single event recorded by several profiles, the standard deviation of the mean is a more appropriate measure of uncertainty; the standard error is typically between 1 and 4%.

For the conditions of interest, the factor  $(E/RT)^2$  is ca. 1000, such that even though the uncertainty on L is much larger than those on E, T, and  $\ln[D_0]$ , all terms are potentially important. Even if  $\sigma_T$  is chosen to be 2 or 3 times larger than our choice, its effect on the final uncertainty is relatively minor, and the contributions of uncertainties on E,  $\ln[D_0]$  and L dominate. For  $(\sigma_E/E) = 4.4\%, (\sigma_T/T) = 1.5\%, (\sigma_L/L) = 50\%, \text{ and } \sigma_{\ln[D0]} = 1.2,$ the uncertainty on t becomes  $(\sigma_t/t) = 215\%$ ; for  $(\sigma_L/L) = 5\%$ ,  $(\sigma_t/L) =$ t) = 190%. Even if  $(\sigma_L/L)$  could be improved,  $(\sigma_E/E)$  and  $\sigma_{\ln[D0]}$ are such that the total uncertainty would not be better than  $\sim$ 190%, showing that our estimates are of appropriate precision for evaluating the parameters of interest. Furthermore, even though these uncertainties are large, our knowledge of the timescales being investigated is minimal, and the estimates remain meaningful. Importantly, none of the conclusions drawn are affected by the particular choice of parameters used.

*Relaxation times and growth rates.* We focus here on core-interior contact residence times, while results for interior-rim contacts, which have been previously studied [31,38], will be detailed elsewhere. These core-interior contact residence times mark – to a good approximation – the onset of crystallization of individual quartz crystals; this is true regardless of how complex the crystallization history may have been (e.g. affected by resorption events), as long as magmatic temperatures were sustained; our calculations are robust provided the boundary conditions used are valid.

Core-interior contact residence times were estimated primarily using Ti profiles of a selected number of crystals, but also using CL images of other crystals. The most important results are shown in Fig. 1 and Table 1. Typical values for the core-interior residence times are 500–1,000 years, for crystals ca. 1 mm wide (Fig. 1a–b). The largest calculated time is that shown in Fig. 1c, i.e.  $\sim$ 2,700 years, for a crystal ca. 2 mm wide. Our analysis suggests that uncertainties are close to 200%, leading to a 95% confidence interval with upper bound close to 13,000 years for the maximum time we estimate, and more typically <5,000 years.

Our core-interior contact residence times are 1-2 orders of magnitude larger than – and thus consistent with – the quartz riminterior residence times of Wark et al. [31]. They are, however, inconsistent with the results of Morgan & Blake [38], who calculate sanidine rim-interior residence times of ~200 ka; more recent data on quartz and sanidine zoning [19,31] shows zoning profiles that are much sharper than those of Anderson et al. [18] used by Morgan & Blake [38], putting into question their calculated timescales.

Importantly, because the growth distance is known for the interior regions, the contact residence times can be used to constrain average growth rates, an important parameter for which estimates are entirely lacking for quartz in large-volume silicic systems like the Bishop Tuff. The agreement between the interior growth rates is remarkable, with all estimates close to  $10^{-14}$  m/s (Fig. 1; Table 1). These values fall within the constraints placed by the analysis of Anderson et al. [18], and are also in good agreement with growth rates for plagioclase phenocrysts in much smaller dacitic systems [39]. The agreement between these growth rates suggests that the crystallization process was rather monotonic, with no sharp discontinuities due to recharging and resorption events – which is consistent with the evidence for phenocryst homogeneity within individual pumice clasts of the Bishop Tuff [6].

**Melt inclusion faceting times.** Quartz crystals from the Bishop Tuff are rich in melt inclusions (now glass), which have been extensively studied by Anderson and co-workers (e.g. [18,24,25]), among others (e.g. [30]). One striking observation is that melt inclusions show a variety of shapes, from round to faceted, sometimes within the same crystal (Fig. 2). For instance, Anderson et al. [18] observed that "Several late-erupted quartz phenocrysts have clear, faceted inclusions located far from crystal rims and round, brown inclusions near the rims of the same crystals". Their observations are suggestive of shape maturation (Fig. 3), during which initially round melt inclusions gradually become faceted (i.e. assume negative crystal shapes) by dissolution and reprecipitation [40–42].

Importantly, many of the larger central melt inclusions are round [18], indicating that only smaller melt inclusions became faceted. This coexistence of round and faceted melt inclusions reveals that the timescale of melt inclusion faceting is similar to the residence time of quartz hosts. Faceting depends on diffusion [42], particularly of Si atoms in the case of quartz, such that significant faceting occurs only at relatively high (i.e. magmatic) temperatures. Hence, determination of melt inclusion faceting times ultimately provides an independent assessment of the longevity of the Bishop magma.

Kinetics of melt inclusion faceting. Melt inclusion faceting is the result of surface free energy minimization. Faceting can be spontaneous if the increase in total surface area – due to conversion from spherical to polyhedral shape – is more than compensated by the accompanying reduction in specific surface energy due to replacement of curved surfaces by flat surfaces [43]. The kinetics of melt inclusion faceting has not been treated in detail, and a full treatment is beyond the scope of this presentation. What we seek is a simplified treatment that can reveal an order of magnitude **Table 1.** Residence times of internal contacts, widths, growth times and growth rates of selected quartz crystals (two of which shown in Fig. 1), as derived from Ti traverses.

CRYSTAL		CORE-INTERIOR CONTACT				
Label	Fig. 1	Residence time <sup>a</sup>	Interior width	Interior growth time <sup>b</sup>	Interior growth rate <sup>c</sup>	
		(years)	(μ <b>m)</b>	(years)	$(10^{-14} m/s)$	
F815-Qtz-17	(a)	775 [3747]	400	765	1.5 [0.3]	
lbA1-Qtz-503	(b)	923 [4461]	334	922	1.0 [0.2]	
lbA1-Qtz-518		512 [2477]	260	506	1.3 [0.3]	

<sup>a</sup>Quantity in brackets is the maximum residence time: t+2 $\sigma_t$ .

<sup>b</sup>Interior growth time excludes the time estimated for the residence time for rim-interior contacts in crystals with bright-CL, high-Ti rims (Gualda et al., unpublished data); these times are short enough that interior growth rates would be unaltered even if they were neglected.

<sup>c</sup>Quantity in brackets is the minimum growth rate obtained using t+2 $\sigma_t$  as time.

doi:10.1371/journal.pone.0037492.t001

assessment of the time required for melt inclusion faceting and, consequently, of the residence times for quartz crystals in the Bishop magma.

We note that the problem involves lateral diffusion of material from the spherical cap that is gradually dissolved into the corner region that progressively forms by reprecipitation (Fig. 3b). We use the volume of the spherical cap that sticks out of the flat surface of the polyhedron of same volume as an estimate of the total volume that needs to be diffused; this is a limiting case that yields maximum faceting time, as the equilibrium shape may be a rounded – rather than a perfect – polyhedron [44]. We then use Fick's first law in combination with the Thomson-Freundlich equation to derive an approximate kinetic expression – similar to the solution for coarsening of a single particle in a matrix [45].

The volume change  $\Delta V$  can be calculated as the volume of the 12 spherical caps that stick out of the flat surfaces of a hexagonal bipyramid of side a and height h:

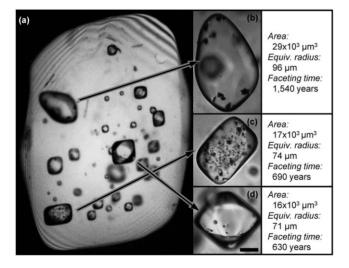


Figure 2. Examples of melt (glass) inclusions in quartz at different stages of faceting. (a) Quartz crystal in refractive index oil (cross-polarized light) showing several melt inclusions. (b–d) Detailed views of the three largest inclusions; scale bar is 50  $\mu$ m and applies to all 3 images; area, radius (of a circle with same area), and faceting time are indicated for each inclusion. Note that (b) is non-faceted, (c) is partly faceted, and (d) is faceted. That only (d) is faceted suggests that crystal residence times are <1,500 years. Images (a–d) are from Anderson et al. [18], reproduced with permission.

doi:10.1371/journal.pone.0037492.g002

$$\Delta V = 4\pi (r - d)^2 (2r + d)$$
(4)

where r is the radius of the sphere and d is the distance between the center of the bipyramid and a flat surface, given by:

$$d = h \frac{\sqrt{3}}{2} \left( \frac{h^2}{a^2} + \frac{3}{4} \right)^{-\frac{1}{2}}$$
(5)

Because we assume equal volumes for the bipyramid and the sphere, we find that:

$$a = \left(\frac{4\sqrt{3}}{9}\pi \frac{a}{h}\right)^{\frac{1}{3}}r$$
(6)

which shows that the volume to be diffused depends only on the size of the original inclusion (r) and the ratio a/h. For quartz, we use a value of 0.909 for a/h.

The flux equation simply states that material transport is by

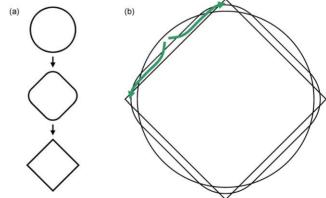


**Figure 3. Shape evolution due to melt inclusion faceting.** (a) Shape change of a melt inclusion inside a host crystal as a function of time due to faceting; initial inclusion is spherical, but with time gets transformed into a polyhedron with rounded edges; with sufficient time, inclusion may become a perfect anticrystal. (b) Evolution of shapes emphasizing the role of diffusion (green arrows) in transporting material to achieve faceting.

doi:10.1371/journal.pone.0037492.g003

$$\frac{dV}{dt} = JA = -D\frac{\Delta C}{r}4\pi r^2$$
(7)

where V is volume, t is time, J is the flux of material per unit area and A is the area of the particle such that JA is the total flux of material through the surface of the particle, D is the diffusion coefficient, and  $\Delta C$  is the concentration difference that drives the process – in units of mass or mol fraction.

The Thomson-Freundlich equation [46] describes the quantity  $\Delta C$  as a function of particle size:

$$\Delta C = \frac{2C_0 \sigma \Omega}{RT} \frac{1}{r}$$
(8)

where  $C_0$  is the solubility of a particle of infinite radius,  $\sigma$  is the surface energy,  $\Omega$  is the molar volume of the phase of interest, R is the ideal gas constant, and T is temperature.

Combining Equations 7 and 8, and assuming that the scaling is appropriate for non-infinitesimal changes, we can calculate the faceting time as:

$$\Delta t = \frac{-RT}{8\pi DC_0 \sigma \Omega} \Delta V \tag{9}$$

The solution to Equation 9 is plotted in Fig. 4, where we used the somewhat conservative values shown in Table 2.

*Error propagation.* We use error propagation to assess how sensitive the computations are to uncertainties in the various parameters in Equation 9, which results:

$$\left(\frac{\sigma_{t}}{t}\right)^{2} = \left(1 - \frac{E}{RT}\right)^{2} \left(\frac{\sigma_{T}}{T}\right)^{2} + \left(\frac{E}{RT}\right)^{2} \left(\frac{\sigma_{E}}{E}\right)^{2} + \left(\frac{\sigma_{V}}{V}\right)^{2} + \left(\frac{\sigma_{C_{0}}}{C_{0}}\right)^{2} + \left(\frac{\sigma_{\sigma}}{\sigma}\right)^{2} + \left(\frac{\sigma_{\Omega}}{\Omega}\right)^{2} + \left(\sigma_{\ln[D_{0}]}\right)^{2}$$

$$(10)$$

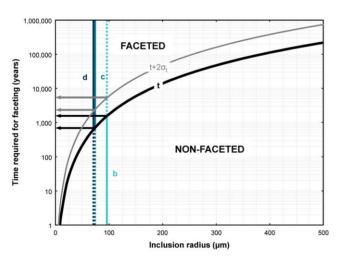


**Figure 4. Melt inclusion faceting time.** Time required for faceting versus inclusion radius plot for conditions relevant for Bishop magma crystallization. Vertical lines correspond to inclusion sizes estimated from Fig. 2. Using our best estimate of faceting time for the observed inclusions, we constrain the timescale for residence of the host crystals to be between ~600–1,500 years. Even if faceting is significantly slower (t+ $2\sigma_t$  curve), residence times are within the range ~2,200–5,300 years. doi:10.1371/journal.pone.0037492.q004

**Table 2.** Parameters used and estimated uncertainties for the computation of melt inclusion faceting time as a function of inclusion radius (r).

	х	$\sigma_X$	Unit	σ <sub>X</sub> /X	Source	
r	100	-	10 <sup>-6</sup> m			
$\Delta V$	4.8 10 <sup>-13</sup>	-	m <sup>3</sup>	$\sim \! 10\%^a$		
R	8.31451	-	J/(K·mol)	-		
т	750	15	°C	2%		
C <sub>0</sub>	0.7	$\sim 0.2^{a}$		$\sim 30\%^a$		
σ	0.02	0.01	J/m <sup>2</sup>	50%	[71]	
Ω	23.7	1.0	10 <sup>-6</sup> m <sup>3</sup> /mol	4%	b	
H <sub>2</sub> O	3	-	Wt. %			
Do	25.8		$10^{-9} \text{ m}^2/\text{s}$		[72]	
In[D <sub>0</sub> ]	-17.5	0.70		4%	[72]	
E	126.5	8.5	10 <sup>+3</sup> J/mol	7%	[72]	
D	1.28	1.06	$10^{-14} \text{ m}^2/\text{s}$	83%	[72]	
(E/RT) <sup>2</sup>	132.6		•	•	•	
Δt	1,242	1,260	а	101%		

<sup>a</sup>Approximate values.

<sup>b</sup>Calculated using the CORBA Phase Properties applet (http://ctserver.ofmresearch.org/phaseProp.html). Retrieved Nov 12, 2007. Calculations based on data from [73].

doi:10.1371/journal.pone.0037492.t002

For the conditions of interest (Table 2),  $(E/RT)^2 = 138$  and  $(1-E/RT)^2 = 115$ , such that the uncertainties in E and T are of much greater importance than what the values of  $\sigma_X/X$  may suggest. An analysis similar to that carried out above for diffusional relaxation shows that the final error, which is ca. 125%, is dominated by the uncertainties in E and  $\ln[D_0]$ .

Faceting times. Our calculations of faceting times show that melt inclusions with 50, 100, and 175  $\mu$ m radius would become faceted in as little 200, 1,700, and 10,000 years, respectively (Fig. 4). That the largest central melt inclusions are not faceted suggests that quartz residence times in the Bishop magma were well below 10,000 years.

Specific results for the melt inclusions shown in Fig. 2 are also plotted in Fig. 4. The non-faceted inclusion (Fig. 2b), which has an equivalent radius (i.e. radius of a circle with the same area as the inclusion) close to 100  $\mu$ m, suggests that it was entrapped less than 1,500 years before eruption. The faceted and partially faceted inclusions (Fig. 2c–d), on the other hand, with equivalent radii  $\sim$ 70–75  $\mu$ m, suggest residence times in excess of  $\sim$ 600 years.

Even if, for sake of argument, we assume that t values are underestimated by 250%  $(+2\sigma)$ , our conclusions do not significantly change, as illustrated in Fig. 4. In this case, instead of a residence time of 600–1,500 years, we would infer a residence time of 2,200–5,300 years for the crystal in Fig. 2, and even inclusions with 170 µm radius would become faceted in ca. 10,000 years.

**Crystal size distributions.** Crystal size distributions in rocks are typically characterized by a monotonic decrease in the number density of crystals with size, with numerous small crystals and few large crystals (see [47] and references therein, among many others). Due to this pronounced decrease in crystal number with increasing size, we use bin sizes that increase by a factor of 2 with increasing size, similar to the practice employed in sedimentology; this yields more robust crystal size distributions, in which the uncertainties in each bin size are similar to each other, rather than quickly increasing with size as would happen with equal bin sizes

(for details, see [48]). The crystal size distributions reveal a twostage growth history for quartz and sanidine [17], with crystals  $>200 \ \mu\text{m}$  recording a simple history of growth under small supersaturation (undercooling) with limited nucleation, characteristic of the pre-eruptive crystallization of a giant magma body with large thermal inertia [14]. Both early- and late-erupted Bishop pumice display such trends (Fig. 5) [14,16,17]. As long as growth rates can be inferred, quartz crystal size distributions yield additional information on the timescales of crystallization [47], and also provide clues to the significance of these timescales.

Theoretical and observational considerations [47] provide compelling evidence that the usual exponential trends (linear in semi-log plots of population density versus size) require linear

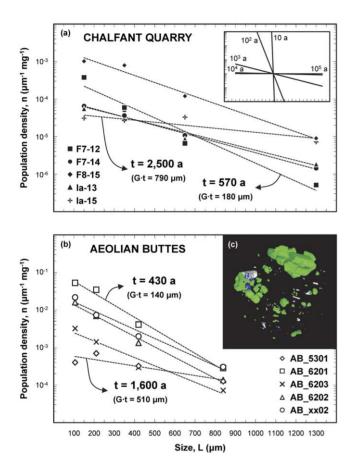


Figure 5. Crystal size distributions. (a) Whole-quartz crystal size distributions for pumice from Chalfant Quarry, obtained by a crushing, sieving and winnowing procedure (data from [14]). (b) Quartz+feldspar crystal size distributions for pumice from Aeolian Buttes, obtained by xray tomography (data from [16,17]). (c) 3D view of pumice chip (sample AB-6203F), showing euhedral quartz and feldspar grains (green), magnetite (blue), and pyroxene±biotite (white); notice the overall trend of decreasing numbers of crystals with increasing size; sample is approximately cylindrical, field of view ~9 mm (see Movie S1 for animated version). In (a) and (b), only crystals larger than 35 µm are shown. Crystal size distributions are well-approximated by exponential distributions (dashed lines). Using growth rates of  $\sim 10^{-14}$  m/s (as calculated above), we calculate crystallization times between 430 and 2,500 years, as indicated; only maximum and minimum estimates shown. Inset in (a) shows slopes of distributions with crystallization times of 10–100,000 years (for  $G = 10^{-14}$  m/s), demonstrating that crystallization times in excess of 10,000 years would yield effectively horizontal size distributions at the scale used, in contrast with the crystal size distributions obtained by us. doi:10.1371/journal.pone.0037492.g005

growth rates with time, as inferred above using relaxation times. That being the case, the largest crystals present are the oldest, and knowledge of growth rates and maximum crystal size leads to estimates of crystal growth time. While determination of maximum size is plagued by extremely incomplete sampling of the existing  $>600 \text{ km}^3$  of erupted magma, crystal size distributions provide constraints on the abundance of such unlikely large crystals. Our data suggest that crystals up to 2 mm in diameter comprise at least 95% of the total crystal mass, and crystals larger than 3 mm (none found in our samples) are exceedingly rare, corresponding to <0.1% of the crystal mass. The growth rates above imply maximum growth times of less than 5,000 years even for 3 mm crystals, such that >99% of the observed crystallization would take place within this time frame.

Additional evidence for the timescales of quartz crystallization derive from crystal size distributions, given that the slope in semilog space decreases systematically with time [47,49]:

$$\ln(\mathbf{n}) = -\frac{1}{Gt}\mathbf{L} + \ln(\mathbf{n}_{o}) \tag{11}$$

where n is population density (i.e. number of crystals per mass per bin size), L is size, G is crystal growth rate (in length per time) and  $n_o$  is the intercept at L = 0. We calculate best-fit exponential curves to quartz crystal size distributions for pumice from Chalfant [14] and to quartz+feldspar size distributions for pumice from Aeolian Buttes [16,17]; using the growth rates calculated above, we infer a duration of the crystallization event between 400 and 2,500 years (Fig. 5) [17].

Our calculations based on crystal size distributions thus suggest residence times for quartz crystals in the millennial scale, in remarkable agreement with our estimates based on diffusional relaxation and melt inclusion faceting, lending confidence to our results. Due to the simultaneous saturation in quartz and two feldspars characteristic of the Bishop magma (see below), this time frame also includes the vast majority of feldspar crystallization, leading to the conclusion that the Bishop existed as a largevolume, crystal-poor magma body for a maximum of only a few thousand years.

#### Thermodynamic and heat flow modeling

Different lines of evidence presented above suggest that quartz crystallization in the Bishop magma lasted only a few thousand years, and most of the crystallization occurred within the final 1,000 years before eruption. One significant question is whether such timescales are consistent with heat flow requirements, i.e. with the need to transport the heat of cooling and crystallization through the country-rocks.

Heat of cooling and crystallization constraints. It has long been argued that the Bishop magma is "eutectoid" in nature (e.g. [18]). In particular for early-erupted Bishop pumice, (1) the coexistence of quartz, sanidine, plagioclase, biotite, magnetite, ilmenite, and a  $H_2O-CO_2$  fluid phase, and (2) the similarity in major-element composition between bulk pumice [6] and melt inclusions in quartz [18] strongly argue for nearly invariant behavior during crystallization.

Using rhyolite-MELTS [23], a modified calibration of MELTS that better predicts the quartz+feldspar saturation surface as a function of pressure, we have simulated the crystallization of representative Bishop compositions under various conditions. In all cases, the expected nearly invariant behavior is well-captured by rhyolite-MELTS (see detailed discussion in [23]); once the system becomes multiply saturated with quartz, sanidine, plagioclase, and fluid, crystallization becomes essentially isothermal, with

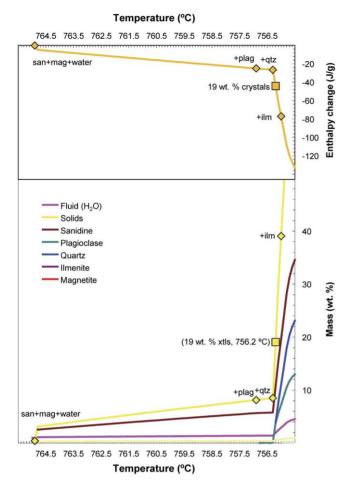


**Figure 6. Thermodynamic and heat flow modeling results.** Temperature (°C) versus enthalpy change (J/g; top panel) and versus abundance (wt. %; bottom panel) plot shows results of MELTS [22,23] simulations. Initial composition is average late-erupted pumice composition from Hildreth [6]. Simulation assumes equilibrium crystallization at 175 MPa, under fluid-saturated conditions (see [23]), in agreement with melt inclusion data [18,24]. Note short crystallization interval (<10°C). Nearly invariant condition is reached at 756.1°C when the system becomes saturated in quartz (in addition to fluid, sanidine, magnetite, and plagioclase), after which point crystallization is nearly isothermal. Quartz crystallization effectively locks the system at the nearly invariant temperature, given that, upon heating, temperature excursions above the nearly invariant temperature are only possible after complete resorption of quartz. doi:10.1371/journal.pone.0037492.q006

>50 wt. % crystallization over less than 1°C (Fig. 6). For earlyerupted Bishop, the 0.5–12 wt. % crystals typically observed in pumice [6,14,50] require <1°C cooling, while late-erupted Bishop can achieve typical 12–25 wt. % crystals in <10°C (Fig. 6).

The importance of this nearly isothermal behavior is that the amount of heat that needs to be withdrawn is essentially limited to latent heat of crystallization, which rhyolite-MELTS calculates to be only 20-30 J/g (see Fig. 6). As a point of comparison, cooling these magmas by  $50^{\circ}$ C would produce an additional  $\sim 65-70$  J/g of heat, making the total amount of heat to be transported 3.5–4 times larger than the nearly isothermal case. Consequently, the nature of the heat-flow problem is significantly influenced by the invariant aspect of crystallization. Furthermore, nearly invariant crystallization effectively locks the system at a fixed temperature, given that temperature excursions are only possible after the

nearly invariant phase (quartz, in this case; see Fig. 6) is completely resorbed.

**Heat flow problem.** Our rhyolite-MELTS simulations not only constrain the total heat of cooling and crystallization required to attain the observed compositions and crystal contents, but also confirm our expectation of nearly invariant crystallization. To contrast the behavior of invariant and non-invariant magmas, we employ well-known analytical solutions [51], which, rather than describing the systems in great detail, capture the essence of the problems of interest.

The Bishop magma body can be reasonably approximated as a 2 km thick body [18,50] losing heat from both top and bottom. Importantly, the evidence accumulated to date for the Bishop Tuff suggests that renewed injections of mafic or felsic magma common in many systems (e.g. [52]) - did not play a major role during crystallization of the Bishop magma body; no direct evidence has been found to date of co-erupted mafic material (e.g. [50]), and felsic magma additions during crystallization are inconsistent with the observed homogeneity of phenocrysts [6], except for late additions [50] possibly connected with the transition towards eruption [31]. Accordingly, we consider a 1 km thick magma column emplaced instantaneously in countryrock at 400°C, with heat loss solely through the top of the column (or, equivalently, a 2 km thick column with heat loss from top and bottom). We explore 3 different solutions (parameters used listed in Table 3):

- (1) Continuous Source (Section 2.4 of [51]). In this case (Fig. 7a), an invariant magma (pure substance or eutectic) is emplaced at the invariant temperature (assumed to be 750°C). Crystallization is dispersed through the melt and the temperature of the magma is kept constant. Heat transport through the magma is fast compared to heat transport through the country-rock. No correction is made for changes in the thermal properties of the magma due to gradual crystallization, but the effect is minimal given the small crystallization interval considered here. Progress of crystallization can be calculated from the heat flux at the boundary, given that all heat lost is latent heat.
- (2) Solidification Front (Section 11.2.IV of [51]). This case (Fig. 7b) is similar to the previous one, except that crystallization takes place along the melt-rock contact. Initially, melt is in direct contact with country-rock, but melt solidifies completely at the contact, and the melt-rock contact migrates inward as crystallization proceeds. While the new solid can have distinct thermal properties, we assume the limiting case in which the thermal properties of the new solid are the same as in the original melt. Progress of crystallization is calculated from the rate of migration of the melt-rock boundary.
- (3) Lovering-type [53]. In this case (Fig. 7c), magma is noninvariant. The effect of latent heat is accounted for by adjusting the specific heat so as to cause latent heat to be released gradually with cooling (see Table 3). In effect, this case is the antithesis of invariant crystallization, with crystallization proceeding linearly with temperature.

Interestingly, solutions (1) and (2) are two end-members of invariant crystallization. In (1), crystallization is dispersed within the melt, with no gradient in crystallinity within the magma, while in (2), melt is always crystal-free and crystallization takes place along the walls. Crystallization of an invariant magma is likely to be intermediate in character between these two models.

**Heat flow and crystallization timescales.** Application of the analytical solutions discussed above (Fig. 7) shows that both

Tab	le	3.	Parameters	used	in	heat-flow	simulations.
-----	----	----	------------	------	----	-----------	--------------

Property	Country rock	Liquid (CGS, °C)	
(Units)	(CGS, °C)		
ρ	2.6 <sup>a</sup>	2.1 <sup>c</sup>	
с	0.21 <sup>a</sup>	0.32 <sup>c</sup>	
к	0.006 <sup>b</sup>	0.0036 <sup>b</sup>	
$\kappa = K/(\rho^*c)$	0.011	0.0058	
L	-	35 <sup>c</sup>	
c <sup>*</sup> = L/50+c	-	1.02 <sup>d</sup>	

"Whittington et al. [74].

<sup>c</sup>Rhyolite-MELTS simulations.

<sup>d</sup>Only for Lovering-type simulation. doi:10.1371/journal.pone.0037492.t003

kinds of invariant crystallization lead to rather quick crystallization, with 25 vol. % crystals being attained within the first 1,000 years of evolution (Fig. 8). In contrast, in the non-invariant case, crystallinity is a function of temperature, and a continuum of crystallinity develops within the magma. Extended periods of time (>10 ka) are needed to start cooling the bottom of the column, by which point  $\sim 1/3$  of the column is fully crystallized, less than half has <25 vol. % crystals, and the bottom of the column is essentially crystal-free. Even for a point lying at half distance from the initial melt-country-rock contact, crystallization rates are much slower than for the invariant case, requiring ca. 8,000 years to attain 25 vol. % crystals (Fig. 8). Not only is non-invariant behavior inconsistent with our rhyolite-MELTS simulations, but the evidence for a continuum in crystal contents is entirely lacking in the Bishop Tuff. And, the relatively narrow range of crystal contents [14,50] and the compositional homogeneity of phenocrysts [6] observed are quite consistent with nearly invariant crystallization.

The contrast in timescales between invariant and non-invariant magmas can be understood based on the differences between the two kinds of heat flow problems. For invariant magmas, all heat loss promotes crystallization, given that there is no sensible heat generation within the magma. Further, with magma temperatures buffered at the invariant temperature, thermal gradients at the magma-rock contact are steeper in the invariant case than the thermal gradients within the magma in the non-invariant case. It results that crystallization proceeds a lot more quickly in the invariant case. That invariant magmas can crystallize as much as 25 vol. % in ca. 1,000 years lends significant support to the timescales of crystallization estimated based on quartz geospeedometry.

# Discussion

#### Implications for the longevity of giant magma bodies

Geospeedometry results suggest quartz crystallization on millennial timescales, and heat flow considerations suggest that these are the expected timescales for the problem of interest. These timescales contrast drastically with radiometric results (e.g. [10]) and with timescales derived from modeling of basalt-to-rhyolite crystallization trajectories using MELTS [54].

Ion probe U-Pb dating suggest zircon crystallization spanned over >100,000 years [10]. In contrast, TIMS U-Pb zircon crystallization ages combined with Ar-Ar eruption ages suggest that zircon crystallization within the final millennia of the Bishop magma history was substantial [11]; these results are contentious

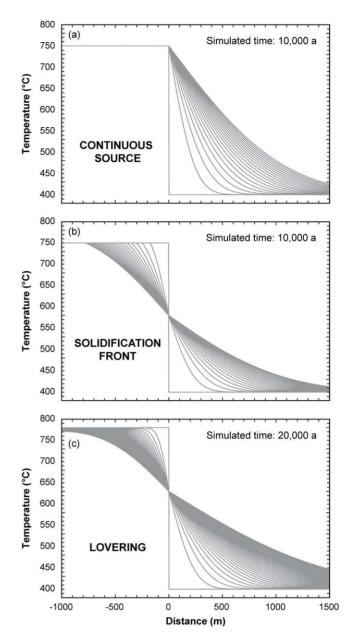
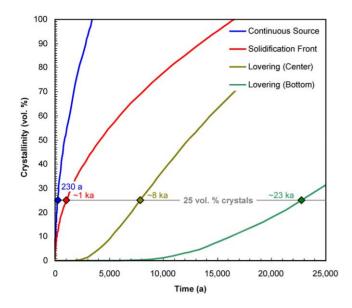


Figure 7. Results of heat-flow simulations showing the thermal evolution of a 1 km thick, semi-infinite magma column. Initial thermal profile is a step-function, with hot (750 or 780°C) magma on the left side and cool (400°C) country-rock on the right side. We use three different analytical solutions: (a) Continuous source, in which crystallization is dispersed throughout the invariant magma, and the magma-country-rock interface is maintained at its original position; changes in the thermal properties of the magma as a function of crystallization are neglected. (b) Solidification front, in which crystallization of invariant magma takes place from the magma-country-rockinterface inward; as a limiting case, thermal properties of the solidified zone are taken to be the same as those of the liquid. (c) Lovering [53], in which the specific heat of the melt (c1) is adjusted so as to simulate crystallization taking place linearly over the course of 50°C cooling; no correction is made to account for changes in thermal properties of initially molten zone as a function of crystallization. Simulation times as indicated; thermal profiles are shown every 500 years. doi:10.1371/journal.pone.0037492.g007

given the difficulties inherent in comparisons of U-Pb and Ar-Ar ages [12], and their potential significance has not been explored. The contrast between these zircon timescales suggests that they are



**Figure 8. Evolution of crystallinity with time for the three solutions presented in Fig. 7 and discussed in the text.** Notice the dramatic differences in behavior between the solutions for invariant magmas (Continuous Source and Solidification Front) and for noninvariant magmas (Lovering). Curves for Lovering-type crystallization are for the center and the bottom of the 1 km column. In particular, notice that significant crystallization (e.g. 25 vol. %) is attained in <1 ka for invariant magmas, in accordance with geospeedometry estimates presented in the text. Much longer timescales are required to cause significant crystallization of the interior of non-invariant magma bodies. doi:10.1371/journal.pone.0037492.g008

in fact recording different facets of the evolution of the Bishop magma. Much of the success in using zircon as a geochronometer stems from its ability to survive through time, but we suspect that it is this unparalleled survival capacity that makes it a poor recorder of the lifetimes of large pools of crystal-poor magma. In order to generate a giant body of crystal-poor magma like the Bishop magma body, it is necessary to partially melt large amounts of crust [55] or to accumulate and crystallize large amounts of parental magma [56], and to segregate this melt from crystal-rich mush, which almost certainly leads to a very dynamic environment characterized by waxing and waning of the melt pool through time [55,57,58]. In such a scenario, it is not surprising that zircon will record a much more protracted history, as slow dissolution rates may limit resorption [59]. Further, zircon extraction from mush may be facilitated by its small size, leading to complex zircon populations [60]. It is thus much more likely that zircon in fact records the construction of these giant bodies of magma (see [61,62] and references therein), which seems to take place over tens to hundreds of thousands of years, in agreement with recent studies of zircon ages in younger volcanic deposits [63,64]. Quartz, on the other hand, records the crystallization of these large masses of segregated evolved melt in hundreds to thousands of years from a virtually crystal-free state.

Crystallization timescales on the order of millions of years have been recently suggested based on MELTS calculations and simple heat balance considerations [54]. Fowler & Spera [54] consider the derivation of high-silica rhyolite from basaltic parental magmas, despite the complete lack of evidence of such derivation, or even for interaction between mafic and felsic magma in the Bishop Tuff. They compute evolution over >400°C, with resulting large changes in melt and mineral compositions, none of which are recorded in Bishop Tuff minerals [6], melt inclusions [18,25], or eruptive products [50]. The significance of their results, in the absence of physical evidence, is thus questionable. On a broad sense, if high-silica rhyolites derive from mafic magmas through step-wise fractionation (e.g. [56]), it is possible that the analysis by Fowler & Spera [54] provides information on the timescales required for fractionation, and it is intriguing that these timescales could be as short as ~130 ka [65], similar to the timescales recorded by zircon. If, on the other hand, high-silica rhyolites are to a significant extent products of crustal recycling (e.g. [55]), then the timescales derived from the exercise conducted by Fowler & Spera [54] are meaningless. In any case, we argue that their analysis does not yield information on the longevity of a large body of crystal-poor rhyolitic magma, which our data strongly suggest to have evolved on millennial timescales.

Our interpretation has fundamental implications. The Bishop magma is characteristically zoned in many respects [6], with this zonation most likely reflecting crystal fractionation processes [66,67]. The homogeneity of phenocryst compositions in individual pumice clasts implies that the magma body zonation predates crystallization [6,50] and was established during emplacement or segregation of magma from a crystal mush. Evidence to date suggests that the Bishop magma was oversaturated in volatiles and contained >15 vol. % pre-eruptive bubbles in its uppermost regions [24]. In this context, the difficulty is not how to trigger a supereruption as much as it is how to prevent one from happening, especially with the timescales inferred from zircon geochronology. With quartz crystallization, bubble exsolution would also occur, with the potential consequence that the system could quickly evolve towards an eruptible state, preventing itself from residing in the crust for extended periods of time. The relatively long repose times – frequently hundreds of thousands of years [3] – observed in many volcanic centers are often taken as an indication of the longevity of giant magma bodies. Short repose times between supereruptions in some areas [68-70] provide circumstantial evidence that giant magma bodies can evolve quickly. In this sense, while zircon geochronometry indicates that it may take hundreds of thousands of years for the crust to be capable of accumulating and segregating large amounts of crystal-poor magma, our data suggest that the giant pools of eruptible magma thus formed are rather ephemeral features, which guickly and effectively destroy themselves during supereruptions.

# Conclusions

We use four lines of evidence to infer the timescales of crystallization of the Bishop Tuff magma body:

- 1. Timescales of relaxation of Ti profiles in quartz suggest quartz residence times of  $\sim$ 500–3,000 years; crystal size distributions suggest that >99 wt. % of crystals present would have crystallized within this timeframe;
- The coexistence of round and partly faceted (negative crystal shape) melt inclusions in quartz suggest that quartz residence times are similar to the timescale for melt inclusion faceting; calculated faceting times suggest quartz residence times of ~500-1,500 years;
- 3. Using growth rates constrained by Ti relaxation times and known crystal sizes, we calculate crystallization times based on crystal size distributions of  $\sim$ 500–2,500 years;
- 4. Thermodynamic considerations suggest crystallization of nearly invariant magma under essentially isothermal conditions; crystallization of such magma would be particularly efficient due to the absence of sensible heat contributions and steep thermal gradients, resulting in crystallization times of <1,000 years.</p>

#### **Supporting Information**

**Movie S1** Animation showing 3D view of crystals in pumice chip (sample AB-6203F). Euhedral quartz and feldspar grains shown in green, magnetite in blue, and pyroxene $\pm$ biotite in white. Note the overall trend of decreasing numbers of crystals with increasing size. Sample is approximately cylindrical, field of view ~9 mm in diameter.

(MPG)

# References

- Self S (2006) The effects and consequences of very large explosive volcanic eruptions. Philosophical Transactions of the Royal Society a-Mathematical Physical and Engineering Sciences 364: 2073–2097.
- Zandt G, Leidig M, Chmielowski J, Baumont D, Yuan XH (2003) Seismic detection and characterization of the Altiplano-Puna magma body, central Andes. Pure and Applied Geophysics 160: 789–807.
- Lowenstern JB, Smith RB, Hill DP (2006) Monitoring super-volcanoes: geophysical and geochemical signals at Yellowstone and other large caldera systems. Philosophical Transactions of the Royal Society a-Mathematical Physical and Engineering Sciences 364: 2055–2072.
- Oppenheimer C (2003) Climatic, environmental and human consequences of the largest known historic eruption: Tambora volcano (Indonesia) 1815. Progress in Physical Geography 27: 230–259.
- Bailey RA, Dalrymple GB, Lanphere MA (1976) Volcanism, structure, and geochronology of Long-Valley Caldera, Mono-County, California. Journal of Geophysical Research 81: 725–744.
- Hildreth W (1979) The Bishop Tuff: Evidence for the origin of compositional zonation in silicic magma chambers. Geological Society of America Special Paper 180.
- Wilson CJN, Hildreth W (1997) The Bishop Tuff: New insights from eruptive stratigraphy. Journal of Geology 105: 407–439.
- Vazquez JA, Reid MR (2004) Probing the accumulation history of the voluminous Toba magma. Science 305: 991–994.
- Charlier BLA, Wilson CJN, Lowenstern JB, Blake S, Van Calsteren PW, et al. (2005) Magma generation at a large, hyperactive silicic volcano (Taupo, New Zealand) revealed by U-Th and U-Pb systematics in zircons. Journal of Petrology 46: 3–32.
- Simon JI, Reid MR (2005) The pace of rhyolite differentiation and storage in an 'archetypical' silicic magma system, Long Valley, California. Earth and Planetary Science Letters 235: 123–140.
- Crowley JL, Schoene B, Bowring SA (2007) U-Pb dating of zircon in the Bishop Tuff at the millennial scale. Geology 35: 1123–1126.
- Renne PR, Mundil R, Balco G, Min KW, Ludwig KR (2010) Joint determination of K-40 decay constants and Ar-40\*/K-40 for the Fish Canyon sanidine standard, and improved accuracy for Ar-40/Ar-39 geochronology. Geochimica Et Cosmochimica Acta 74: 5349–5367.
- Chakraborty S (2008) Diffusion in solid silicates: A tool to track timescales of processes comes of age. Annual Review of Earth and Planetary Sciences 36: 153–190.
- Gualda GAR, Cook DL, Chopra R, Qin LP, Anderson AT, et al. (2004) Fragmentation, nucleation and migration of crystals and bubbles in the Bishop Tuff rhyolitic magma. Transactions of the Royal Society of Edinburgh-Earth Sciences 95: 375–390.
- Gualda GAR, Rivers M (2006) Quantitative 3D petrography using X-ray tomography: Application to Bishop Tuff pumice clasts. Journal of Volcanology and Geothermal Research 154: 48–62.
- Pamukcu AS, Gualda GAR (2010) Quantitative 3D petrography using X-ray tomography 2: Combining information at various resolutions. Geosphere 6: 775–781.
- Pamukcu AS, Gualda GAR, Anderson AT (2012) Crystallization stages of the Bishop Tuff magma body recorded in crystal textures in pumice clasts. Journal of Petrology 53: 589–609.
- Anderson AT, Davis AM, Lu FQ (2000) Evolution of Bishop Tuff rhyolitic magma based on melt and magnetite inclusions and zoned phenocrysts. Journal of Petrology 41: 449–473.
- Gualda GAR (2007) Crystal and bubble populations in the early-erupted Bishop rhyolitic magma: Microscopy, x-ray tomography and microanalysis of pumice clasts [Ph.D. Thesis]: The University of Chicago. 284 p.
- Peppard BT, Steele IM, Davis AM, Wallace PJ, Anderson AT (2001) Zoned quartz phenocrysts from the rhyolitic Bishop Tuff. American Mineralogist 86: 1034–1052.

# Acknowledgments

We thank Ian Steele and Matthew Newville for assistance with analytical work, Bruce Buffet and David Furbish for discussions on diffusion and numerical problems, and Calvin Miller and other MESSY members for suggestions on the manuscript. Reviews by Victoria Smith, Jacob Lowenstern, Jon Blundy and Christian Huber, and suggestions by Olivier Bachmann are greatly appreciated.

# **Author Contributions**

Conceived and designed the experiments: GARG. Performed the experiments: GARG ASP MSG ATA SRS MLR. Analyzed the data: GARG ASP MSG ATA SRS. Contributed reagents/materials/analysis tools: SRS MLR MSG. Wrote the paper: GARG.

- Sutton SR, Bertsch PM, Newville M, Rivers M, Lanzirotti A, et al. (2002) Microfluorescence and microtomography analyses of heterogeneous Earth and environmental materials. Reviews in Mineralogy & Geochemistry 49: 429–483.
- 22. Ghiorso MS, Sack RO (1995) Chemical mass-transfer in magmatic processes. 4. A revised and internally consistent thermodynamic model for the interpolation and extrapolation of liquid-solid equilibria in magmatic systems at elevatedtemperatures and pressures. Contributions to Mineralogy and Petrology 119: 197–212.
- Gualda GAR, Ghiorso MS, Lemons RV, Carley TL (2012) Rhyolite-MELTS: A modified calibration of MELTS optimized for silica-rich, fluid-bearing magmatic systems. Journal of Petrology 53: 875–890.
- Wallace PJ, Anderson AT, Davis AM (1995) Quantification of pre-eruptive exsolved gas contents in silicic magmas. Nature 377: 612–616.
- Wallace PJ, Anderson AT, Davis AM (1999) Gradients in H<sub>2</sub>O, CO<sub>2</sub>, and exsolved gas in a large-volume silicic magma system: Interpreting the record preserved in melt inclusions from the Bishop Tuff. Journal of Geophysical Research-Solid Earth 104: 20097–20122.
- Papale P, Moretti R, Barbato D (2006) The compositional dependence of the saturation surface of H2O+CO2 fluids in silicate melts. Chemical Geology 229: 78–95.
- Tamic N, Behrens H, Holtz F (2001) The solubility of H2O and CO2 in rhyolitic melts in equilibrium with a mixed CO2-H2O fluid phase. Chemical Geology 174: 333–347.
- Holtz F, Becker A, Freise M, Johannes W (2001) The water-undersaturated and dry Qz-Ab-Or system revisited. Experimental results at very low water activities and geological implications. Contributions to Mineralogy and Petrology 141: 347–357.
- Johannes W, Holtz F (1996) Petrogenesis and experimental petrology of granitic rocks. Berlin: Springer. 335 p.
- Hervig RL, Dunbar NW (1992) Cause of chemical zoning in the Bishop (California) and Bandelier (New-Mexico) magma chambers. Earth and Planetary Science Letters 111: 97–108.
- Wark DA, Hildreth W, Spear FS, Cherniak DJ, Watson EB (2007) Pre-eruption recharge of the Bishop magma system. Geology 35: 235–238.
- Thomas JB, Watson EB, Spear FS, Shemella PT, Nayak SK, et al. (2010) TitaniQ under pressure: the effect of pressure and temperature on the solubility of Ti in quartz. Contributions to Mineralogy and Petrology 160: 743–759.
- Morgan DJ, Blake S, Rogers NW, De Vivo B, Rolandi G, et al. (2006) Magma chamber recharge at Vesuvius in the century prior to the eruption of AD 79. Geology 34: 845–848.
- Cherniak DJ, Watson EB, Wark DA (2007) Ti diffusion in quartz. Chemical Geology 236: 65–74.
- Wark DA, Watson EB (2006) TitaniQ: a titanium-in-quartz geothermometer. Contributions to Mineralogy and Petrology 152: 743–754.
- Crank J (1979) The mathematics of diffusion. Oxford: Oxford University Press. pp 13–15.
- Bindeman IN, Valley JW (2002) Oxygen isotope study of the Long Valley magma system, California: isotope thermometry and convection in large silicic magma bodies. Contributions to Mineralogy and Petrology 144: 185–205.
- Morgan DJ, Blake S (2006) Magmatic residence times of zoned phenocrysts: introduction and application of the binary element diffusion modelling (BEDM) technique. Contributions to Mineralogy and Petrology 151: 58–70.
- McCanta MC, Rutherford MJ, Hammer JE (2007) Pre-eruptive and syneruptive conditions in the Black Butte, California dacite: Insight into crystallization kinetics in a silicic magma system. Journal of Volcanology and Geothermal Research 160: 263–284.
- Beddoe-Stephens B, Aspden JA, Shepherd TJ (1983) Glass inclusions and melt compositions of the Toba Tuffs, Northern Sumatra. Contributions to Mineralogy and Petrology 83: 278–287.
- Manley CR (1996) Morphology and maturation of melt inclusions in quartz phenocrysts from the Badlands rhyolite lava flow, southwestern Idaho. American Mineralogist 81: 158–168.

- Chaigneau M, Massare D, Clocchiatti R (1980) Contribution à l'étude des inclusions vitreuses et des éléments volatils contenus dans les phénocristaux de quartz de roches volcaniques acides. Bulletin of Volcanology 43: 233–240.
- 43. Roedder E (1984) Fluid inclusions. Reviews in Mineralogy 12: 59-66.
- Wortis M (1988) Equilibrium crystal shapes and interfacial phase transitions. In: Vanselow R, Howe RF, eds. Chemistry and Physics of Solid Surfaces VII. New York: Springer-Verlag.
- Shewmon PG (1969) Transformations in metals. New York: McGraw-Hill. 301 p.
- 46. Paul A (1990) Chemistry of glasses. New York: Chapman and Hall.
- Marsh BD (1998) On the interpretation of crystal size distributions in magmatic systems. Journal of Petrology 39: 553–599.
   Gualda GAR (2006) Crystal size distributions derived from 3D datasets: Sample
- Guardo GAR (2000) crystal size distributions derived non-5D datasets. Sample size versus uncertainties. Journal of Petrology 47: 1245–1254.
   Marsh BD (1988) Crystal size distribution (CSD) in rocks and the kinetics and
- Marsh BD (1988) Crystal size distribution (CSD) in rocks and the kinetics and dynamics of crystallization .1. Theory. Contributions to Mineralogy and Petrology 99: 277–291.
- Hildreth W, Wilson CJN (2007) Compositional zoning of the Bishop Tuff. Journal of Petrology 48: 951–999.
- Carslaw HS, Jaeger JC (1984) Conduction of heat in solids. Oxford: Oxford University Press. 510 p.
- Annen C (2011) Implications of incremental emplacement of magma bodies for magma differentiation, thermal aureole dimensions and plutonism-volcanism relationships. Tectonophysics 500: 3–10.
- Lovering TS (1936) Heat conduction in dissimilar rocks and the use of thermal models. Bulleting of the Geological Society of America 47: 87–100.
- Fowler SJ, Spera FJ (2010) A Metamodel for Crustal Magmatism: Phase Equilibria of Giant Ignimbrites. Journal of Petrology 51: 1783–1830.
- Bindeman IN, Fu B, Kita NT, Valley JW (2008) Origin and evolution of silicic magmatism at Yellowstone based on ion microprobe analysis of isotopically zoned zircons. Journal of Petrology 49: 163–193.
- Bachmann O, Bergantz GW (2004) On the origin of crystal-poor rhyolites: Extracted from batholithic crystal mushes. Journal of Petrology 45: 1565–1582.
- Walker BA, Miller CF, Claiborne LL, Wooden JL, Miller JS (2007) Geology and geochronology of the Spirit Mountain batholith, southern Nevada: Implications for timescales and physical processes of batholith construction. Journal of Volcanology and Geothermal Research 167: 239–262.
- Mahood GA (1990) Evidence for long residence times of rhyolitic magma in the Long Valley magmatic system - The isotopic record in the precaldera lavas of Glass Mountain - Reply. Earth and Planetary Science Letters 99: 395–399.
- Watson EB (1996) Dissolution, growth and survival of zircons during crustal fusion: Kinetic principles, geological models and implications for isotopic inheritance. Transactions of the Royal Society of Edinburgh-Earth Sciences 87: 43–56.

- Simon JI, Reid MR, Young ED (2007) Lead isotopes by LA-MC-ICPMS: Tracking the emergence of mantle signatures in an evolving silicic magma system. Geochimica Et Cosmochimica Acta 71: 2014–2035.
- Miller JS, Matzel JEP, Miller CF, Burgess SD, Miller RB (2007) Zircon growth and recycling during the assembly of large, composite arc plutons. Journal of Volcanology and Geothermal Research 167: 282–299.
- Storm S, Shane P, Schmitt AK, Lindsay JM (2011) Contrasting punctuated zircon growth in two syn-erupted rhyolite magmas from Tarawera volcano: Insights to crystal diversity in magmatic systems. Earth and Planetary Science Letters 301: 511–520.
- Schmitt AK, Stockli DF, Lindsay JM, Robertson R, Lovera OM, et al. (2010) Episodic growth and homogenization of plutonic roots in arc volcanoes from combined U-Th and (U-Th)/He zircon dating. Earth and Planetary Science Letters 295: 91–103.
- Claiborne LL, Miller CF, Flanagan DM, Clynne MA, Wooden JL (2010) Zircon reveals protracted magma storage and recycling beneath Mount St. Helens. Geology 38: 1011–1014.
- Gualda GAR, Ghiorso MS (2011) Comment on 'A metamodel for crustal magmatism: Phase equilibria of giantignimbrites' by S. J. Fowler and F. J. Spera. Journal of Petrology 52: 431–434.
- Michael PJ (1983) Chemical differentiation of the Bishop Tuff and other highsilica magmas through crystallization processes. Geology 11: 31–34.
- Miller CF, Mittlefehldt DW (1984) Extreme fractionation in felsic magma chambers - A product of liquid-state diffusion or fractional crystallization. Earth and Planetary Science Letters 68: 151–158.
   Lipman PW, McIntosh WC (2008) Eruptive and noneruptive calderas,
- Lipman PW, McIntosh WC (2008) Eruptive and noneruptive calderas, northeastern San Juan Mountains, Colorado: Where did the ignimbrites come from? Geological Society of America Bulletin 120: 771–795.
- Pabst S, Worner G, Civetta L, Tesoro R (2008) Magma chamber evolution prior to the Campanian Ignimbrite and Neapolitan Yellow Tuff eruptions (Campi Flegrei, Italy). Bulletin of Volcanology 70: 961–976.
- Wilson CJN, Charlier BLA (2009) Rapid Rates of Magma Generation at Contemporaneous Magma Systems, Taupo Volcano, New Zealand: Insights from U-Th Model-age Spectra in Zircons. Journal of Petrology 50: 875–907.
- Dowty E (1980) Crystal growth and nucleation theory and the numerical simulation of igneous crystallization. In: Hargraves RB, ed. Physics of magmatic processes. Princeton, N.J.: Princeton University Press.
- Baker DR (1991) Interdiffusion of hydrous dacitic and rhyolitic melts and the efficacy of rhyolite contamination of dacitic enclaves. Contributions to Mineralogy and Petrology 106: 462–473.
- Berman RG (1988) Internally-consistent thermodynamic data for minerals in the system Na<sub>2</sub>O-K<sub>2</sub>O-CaO-MgO-FeO-Fe<sub>2</sub>O<sub>3</sub>-Al<sub>2</sub>O<sub>3</sub>-SiO<sub>2</sub>-TiO<sub>2</sub>-H<sub>2</sub>O-CO<sub>2</sub>. Journal of Petrology 29: 445–522.
- Whittington AG, Hofmeister AM, Nabelek PI (2009) Temperature-dependent thermal diffusivity of the Earth's crust and implications for magmatism. Nature 458: 319–321.